PHYSICAL REVIEW D

PARTICLES AND FIELDS

THIRD SERIES, VOLUME 36, NUMBER 6 15 SEPTEMBER 1987

Comparison of bar and interferometer sensitivities to sources of transient gravitational radiation

Daniel Dewey

Massachusetts Institute of Technology, Cambridge, Massachusetts 02139

(Received 1 April 1987)

The signal-to-noise ratios for the detection of gravitational radiation are derived and compared for resonant bar and laser interferometric detectors. The results presented here apply to the detection of transient gravitational radiation as would be emitted in particle–black-hole interactions, stellar collapse events, or the decay of compact binary systems. For the detection of fixed-energy gravitational-wave bursts, the bar antenna shows its resonant nature with a sensitivity that is broadly peaked near the bar frequency, while the interferometer response shows a smooth f^{-1} dependence. Applied to the detection of the radiation emitted in the decay of a compact binary system, the ratio of bar to interferometer sensitivities is independent of source parameters. Using operational antenna parameters (circa 1985), the 4.2-K Stanford bar ($T_d = 20$ mK, $M_a = 4.8 \times 10^3$ kg, $L_a = 3$ m, $f_a = 840$ Hz) is shown to be typically three times more sensitive to transient sources than the 30-m interferometer ($\tilde{h} = 2 \times 10^{-19}/\sqrt{\text{Hz}}$ above 500 Hz) at the Max-Planck-Institut für Quantenoptik in Garching, West Germany. Additionally, the signal-to-noise ratios calculated here are normalized to represent optimistic Galactic sources (located at 10 kpc, $10^{-2}\, M_\odot c^2$ emitted in a gravitational burst) and indicate that both antennas are operating near astrophysically interesting sensitivities with signal-to-noise ratios ranging from 1 to 10 for these sources.

I. INTRODUCTION

The development of antennas for the detection of gravitational radiation has lead to two basic antenna designs: resonant bar antennas[1,2] and laser interferometric antennas.[3–5] Much work has gone into an analysis of the operation of these detectors; however, a detailed comparison of the sensitivities of these two antenna types has not been carried out. The goal of this paper is to present a complete and realistic comparison of bar and interferometer detector sensitivities. The new results of this comparison stem from including explicit wave shapes for the gravitational radiation, evaluating the bar response for the given waveform, and using the matched filter signal-to-noise ratio (SNR) in evaluating the interferometer response; the seeds of many of these ideas appear in Weiss.[4] In addition, the SNR's are evaluated for optimistic Galactic sources in order to put the sensitivities of the current antennas in an astrophysical perspective.

The predicted sources of gravitational radiation can be divided into two basic categories: continuous and transient sources. This work deals with the transient sources which include stellar collapse events, particle–black-hole events, and the final swept-frequency waveform, or chirp, expected in decaying compact binary systems, e.g., neutron-star binaries such as PSR1913 + 16 (Ref. 6). This comparison, then does not consider periodic nor stochastic sources whose waveforms are (humanly) infinite in duration. Note that some systems can be viewed, during the course of their lifetime, as sources of both transient and continuous radiation.

The operation of the antennas can be described in one theoretical framework[7] in which the gravitational radiation induces time-dependent tidal forces in the detector mass(es). The results of these forces are motions which must be detected in the presence of a variety of noise terms. In practice, however, the present antenna types respond in different ways to gravitational radiation and are limited by different noise sources. In particular, the bar antennas respond to $\dot{h}(t)$ with a limiting detection noise energy kT_d ideally set by the bar thermal noise, while the interferometric antennas measure $h(t)$ in the presence of a white strain noise $\tilde{h}$ due to the laser shot noise.

In order to realistically compare the sensitivities of the antennas, suitable models for the response and noise levels of each antenna type are required. In addition, waveforms representative of those likely to be detected must be used in the comparison. These ingredients are presented in Secs. II and III for the sources, and in Secs. IV and V for the antennas. Finally, in Secs. VI and VII, a comparison of two representative antennas, the Stanford bar and the

Max-Planck-Institut für Quantenoptik, Garching, West Germany (MPQ Garching) interferometer, is made and the results are discussed.

II. PREDICTED BURST WAVEFORMS

The burst sources, a subset of the transient sources, include particle–black-hole encounters and stellar collapse events. Much theoretical work has been devoted to modeling these systems and predicting gravitational-wave shapes and amplitudes;[8–13] some examples of the results of the theoretical calculations are shown in Fig. 1. As can be seen here, both types of systems have predicted gravitational waveforms $h(t)$ consisting of from 1 to perhaps 10 or more half-cycles at a roughly well-defined frequency. The burst wave shape, its frequency, and its amplitude are all a function of the parameters of the source.

Particle–black-hole systems are parametrized by the test-particle mass μ and its orbital angular momentum, and by the black-hole mass M and its Kerr parameter. Calculations show that gravitational radiation is emitted at a frequency of order 10 kHz$\times M_\odot/M$, and the total energy emitted in gravity waves is given by a constant times $\mu c^2 \mu/M$, where this constant can vary from 10^{-2} (or less) to 1 (Ref. 8). The number of half-cycles in the emitted waveform is of order 1 for the case of radial infall, but can be as many as 10 if the particle is scattered around and from the, possibly rotating, black hole. Because of the wide mass range over which black holes might exist, gravitational radiation from these sources is expected anywhere below 10 kHz. A typical event detectable by antennas operating in the 100 Hz–10 kHz range might have $\mu = 1M_\odot$, $M = 10M_\odot$, and emit a total energy of $10^{-2}M_\odot c^2$ at 1 kHz.

Stellar collapse events, in particular type-II supernovas, are somewhat more constrained in their emission frequency, as progenitors span a less wild parameter space, with masses typically $10–20M_\odot$. However, the dynamics of the core provide for a variety of possible waveforms with shapes ranging from a single half-cycle, as in Fig. 1(f), to many cycles as in the case of the oscillating core of Fig. 1(e). As in the particle–black-hole case, the frequency scale is roughly 10 kHz$\times M_\odot/M$ and emission efficiencies[9] can be of order 10^{-3}. An optimistic source may have $M = 10M_\odot$, producing a waveform with a frequency at about 1 kHz and an emitted energy of $E \sim 10^{-2}M_\odot c^2$.

For analytic simplicity, most of the waveforms for stellar collapse and particle–black-hole events can be approximated by a canonical set of finite-length sinusoidal waveforms. The parameters of these waveforms are the frequency $\omega_g = 2\pi f_g$, the length of the burst measured in half-cycles $N_{\rm hc}$, and the amplitude h_0 of the waveform. These parameters are explicitly defined in Fig. 2, where a canonical burst waveform $h(t)$ is shown as well as its second time derivative $\ddot{h}(t)$. Analytically these waveforms are given by

$$h(t) = h_0 \sin(\omega_g t) W\left[0, \frac{N_{\rm hc}\pi}{\omega_g}, t\right] \tag{1}$$

and

$$\ddot{h}(t) = -h_0 \omega_g{}^2 \sin(\omega_g t) W\left[0, \frac{N_{\rm hc}\pi}{\omega_g}, t\right] + \omega_g h_0 \left[\delta(t) - (-1)^{N_{\rm hc}} \delta\left[t - \frac{N_{\rm hc}\pi}{\omega_g}\right]\right], \tag{2}$$

where the window function W is defined as

$$W(t_1, t_2, t) = \begin{cases} 1 & \text{for } t_1 < t < t_2 , \\ 0 & \text{otherwise} . \end{cases}$$

Note that the differentiation of $h(t)$ has produced two δ-function terms in $\ddot{h}(t)$ which arise from the slope discon-

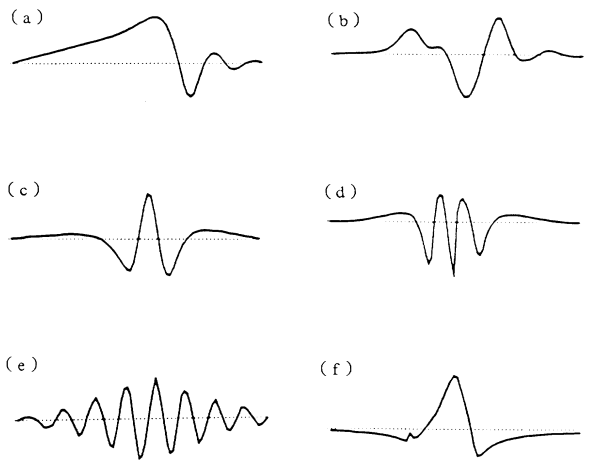

FIG. 1. Wave shapes representative of the gravitational radiation expected from burst sources. The wave shapes shown here are digitized versions of published theoretical predictions for a variety of systems: (a) a test particle falling radially into a Schwarzschild black hole (Ref. 8); (b) rotating stellar collapse (Ref. 9); (c) a test particle scattered from a Kerr black hole (Ref. 10); (d) a test particle from a Schwarzschild black hole (Ref. 11); (e) damped ellipsoidal stellar collapse (Ref. 12); and (f) cold rotating stellar collapse (Ref. 13).

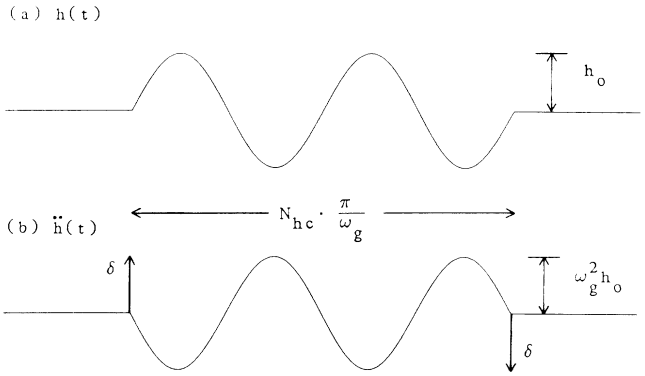

FIG. 2. Canonical $h(t)$ burst waveform and its second time derivative. These waveforms are parametrized by the burst frequency $\omega_g = 2\pi f_g$, the number of half-cycles in the burst $N_{\rm hc}$, and the burst amplitude h_0. They are used to analytically evaluate the response of the antennas to burst sources of gravitational radiation.

tinuities in the canonical waveform. In "real" waveforms "wings" or "tails" will be present; approximating these by the δ functions will introduce negligible errors in the response calculations of Sec. V.

The parameter h_0, above, sets the amplitude of the gravitational wave, and, as such, does not affect the comparison of the detector types. However, to put the antenna responses into a realistic astrophysical context, we can normalize the amplitude of the waveform so that it represents the emission of a constant amount of gravitational-wave energy. The energy flux of a gravitational wave is proportional to $\int \dot{h}^2(t)$ (Ref. 7); assuming that the same flux is radiated in all directions the total energy radiated is

$$E_{\text{total}}=\epsilon Mc^2=4\pi R^2\frac{c^3}{16\pi G}\int \dot{h}^2(t)dt \simeq 4\pi R^2\frac{c^3}{16\pi G}\omega_g{}^2\int h^2(t)dt \ . \quad (3)$$

Here E_{total} is also expressed as an efficiency ϵ times an energy characteristic of the system Mc^2. Values of E_{total} and R, chosen for optimistic sources in the Galaxy, are $E_{\text{total}}=0.01M_\odot c^2$ and $R=R_{GC}\sim 10$ kpc. Substituting Eq. (1) into Eq. (3), the corresponding value of h_0 for the canonical waveform is given by

$$h_0=\frac{1}{R}\left[\epsilon M\frac{8G}{c}\right]^{1/2}(N_{\text{hc}}\omega_g)^{-1/2} \simeq 8\times 10^{-18}\left[\frac{\epsilon M}{10^{-2}M_\odot}\right]^{1/2}\left[\frac{1\text{ kHz}}{f_g}\right]^{1/2}N_{\text{hc}}{}^{-1/2} \ . \quad (4)$$

For this choice of h_0, the signal-to-noise ratios calculated in Sec. VI below are not only useful in *comparing* bar and interferometer sensitivities, but they also give an indication of the *absolute* sensitivity of the current detectors to (optimistic) galactic gravitational burst sources.

III. THEORETICAL CHIRP WAVEFORMS

This source has received much attention because of the existence of PSR1913 + 16 and the source's clean analytic behavior; two works are particularly illuminating in the context of the emission and detection of gravitational radiation from this system. One by Forward and Berman[14] was written before neutron-star binaries were discovered; and the second, by Clark and Eardley,[15] covers these systems in more astrophysical depth than is possible here. The presentation below summarizes the equations governing the gravitational radiation emitted by this system.

Assuming a source orientation which has its orbital plane perpendicular to the line of sight, the waveform emitted by the binary system is sinusoidal with a frequency and amplitude increasing in time; this sweep in frequency is responsible for the "chirp" appellation.[14] In finite time the system will decay to coalescence, and, thus, the system state can be parametrized by the time to coalescence τ; note that $d\tau/dt=-1$. Using this parametrization, the frequency of gravitational radiation, twice the orbital frequency, is given by

$$\omega_g(\tau)=2\left[\frac{256}{5}\frac{G^{5/3}}{c^5}\right]^{-3/8}F^{-3/8}\tau^{-3/8} \ , \quad (5)$$

and, evaluating the quadrupole formula[16] for masses in a circular orbit, the corresponding amplitude of the emitted gravitational radiation is

$$h_{\text{amp}}(\tau)=\frac{1}{R}\left[\frac{5G^5}{c^{11}}\right]^{1/4}F^{3/4}\tau^{-1/4} \ , \quad (6)$$

where

$$F\equiv\frac{m_1m_2}{(m_1+m_2)^{1/3}}=\mu(m_1+m_2)^{2/3}=\mu m_T{}^{2/3} \ . \quad (7)$$

Thus, both the waveshape and the amplitude are determined by two parameters: one a function of the system masses $F(m_1,m_2)$ and the other the separation of the source and antenna R. Note that unlike the burst sources, no assumptions about efficiency are required. (This unique property has led to the interesting proposal that observation of these sources could be used to determine the Hubble constant.[17])

Equation (5) for ω_g can be integrated to yield an expression for the amount of phase remaining until coalescence

$$\phi(\tau)=\tfrac{16}{5}\left[\frac{256}{5}\frac{G^{5/3}}{c^5}\right]^{-3/8}F^{-3/8}\tau^{5/8} \ . \quad (8)$$

Note that even though ω_g approaches infinity as τ goes to zero, the total phase is finite due to the gentle $\tau^{-3/8}$ dependence of ω_g. Using this phase the $h(t)$ waveform can be readily approximated by

$$h(\tau)=h_{\text{amp}}(\tau)\sin[\phi(\tau)+\phi_{\text{arb}}] \ , \quad (9)$$

where ϕ_{arb} is an arbitrary initial phase. Because $h_{\text{amp}}(\tau)$ varies slowly compared to the sin term, $\ddot{h}(t)$ is well approximated by

$$\ddot{h}(\tau)=-h_{\text{amp}}(\tau)\omega_g{}^2(\tau)\sin[\phi(\tau)+\phi_{\text{arb}}] \ . \quad (10)$$

With these expressions for the waveforms, the response of the antennas can be calculated and compared.

Before leaving this summary of the chirp source, it is important to note that at some point the real physical system will deviate from the approximate waveforms given above, particularly at small values of τ and large values of ω_g. Even before additional general-relativistic corrections are required, deviations from the assumption of ideal, pointlike masses can become important. In particular, for the case of neutron-star binaries, Roche lobe overflow with possible "immediate tidal disruption" due to runaway mass transfer can halt the decay at high orbital frequencies.[15] These effects are predicted to be important when the separation a of the components is less than several neutron star radii. Using the Newtonian relation for the orbital frequency

$$\omega_{\text{orb}}{}^2=\frac{G(m_1+m_2)}{a^3} \ , \quad (11)$$

the separation of the objects as a function of ω_g is given

by

$$a(\omega_g)=[4G(m_1+m_2)]^{1/3}\omega_g{}^{-2/3} . \quad (12)$$

[Note that this depends on the masses in a form different from Eqs. (5) and (6) above, and, thus, the observation of a complete chirp waveform provides more information than that needed for the determination of F and R only.] Choosing values of $m_1=m_2=1.4M_\odot$ and $a=30$ km, leads to a maximum frequency of 1200 Hz at which point the total remaining phase to coalescence is only about 5 cycles.

Finally, in addition to the astrophysical restrictions on the validity of the chirp equations near coalescence, there are restrictions imposed by the detector analysis schemes. Anticipating the results of Secs. IV and V, the simple analytic detection analyses become inaccurate when there are less than several cycles remaining in the waveform. The frequency at which N cycles remain in the waveform $\omega_{N\mathrm{cy}}$ can be calculated by setting Eq. (8) equal to $2\pi N$ and solving for $\tau_{N\mathrm{cy}}$; then, using Eq. (5), $\omega_{N\mathrm{cy}}$ can be calculated from $\tau_{N\mathrm{cy}}$ with

$$\omega_{N\mathrm{cy}}=2\left[32\pi N\frac{G^{5/3}}{c^5}F\right]^{-3/5} . \quad (13)$$

For the case of $N=5$ this frequency is

$$f_{5\mathrm{cy}}=1525\ \mathrm{Hz}\left[\frac{F_\odot}{F}\right]^{3/5} , \quad (14)$$

where $F_\odot=M_\odot{}^{5/3}$. The antenna analyses will require that $f_{5\mathrm{cy}}$ for the source be comparable to or larger than a threshold frequency characteristic of the detector in order for the SNR's calculated here to be accurate. This requirement is comparable to the astrophysical one given above for the case of a neutron-star binary with $m_1=m_2=1.4M_\odot$; for neutron-star binaries with smaller masses tidal disruption will occur before the system reaches the five-cycle frequency. However, because the five-cycle limit is independent of source models it alone will be used to limit the range of F over which analytic chirp detection results are presented.

IV. INTERFEROMETER: MODEL AND RESPONSE

The output of an interferometric system is a measure of $h(t)$ and the dominant noise term for present-day antennas is a white-noise source $\tilde{h}$ determined principally by the shot noise of the laser light illuminating the interferometer.[18] The maximum signal-to-noise ratio obtainable by a data analysis system searching for this $h(t)$ signal is[19]

$$(S/N)_I=\left[\frac{2\int h^2(t)dt}{\tilde{h}^2}\right]^{1/2} . \quad (15)$$

Note that here and throughout this work an *amplitude* SNR is used; that is to say, if the amplitude of $h(t)$ were doubled then the SNR of a detection would increase by a factor of 2. Equation (15) is valid for a general waveform, and through numerical integration the optimal SNR for

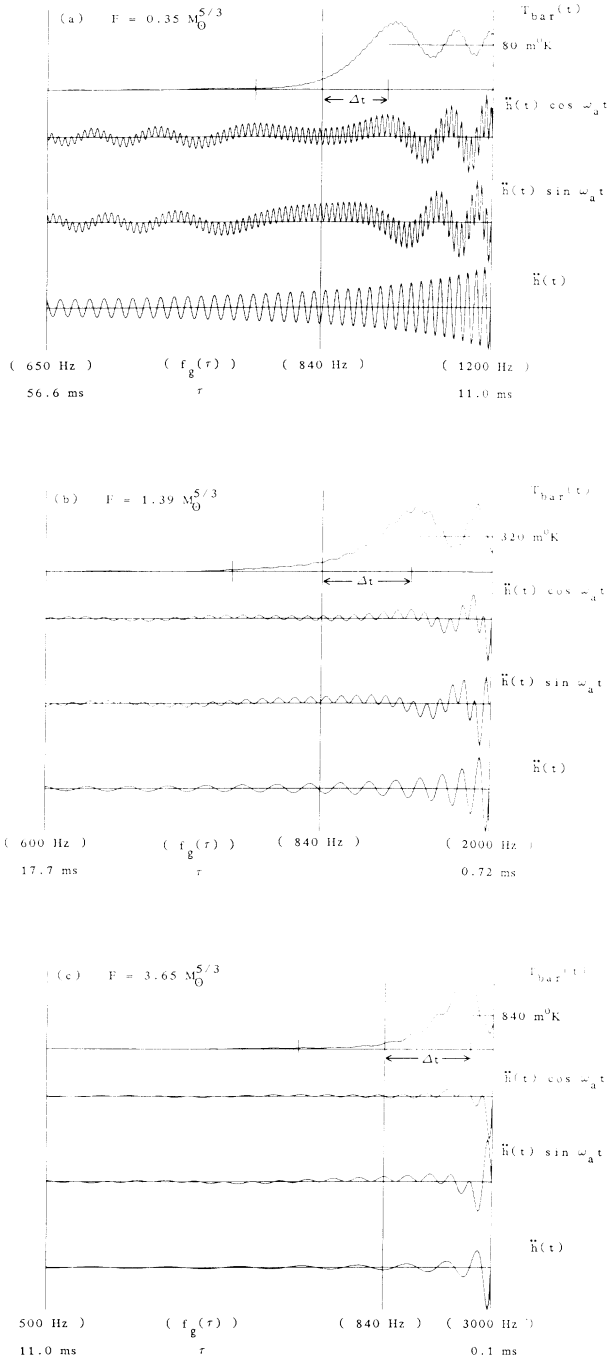

FIG. 3. Numerical simulations of a bar antenna's response to a chirp waveform emitted by a compact binary system, shown for three values of the source parameter $F=\mu m\tau^{2/3}$. Plotted as a function of τ, the time to coalescence, are the $\ddot{h}(t)$ waveform, the integrands of Eq. (21), and the temperature equivalent of the energy deposited in the bar as of time τ. Note that as F increases, the chirp moves to lower frequencies and the number of cycles of the waveform above the bar frequency is reduced. The time Δt indicated is calculated from Eq. (26) and the asymptotic temperatures indicated have been calculated from Eqs. (29) and (18). Other parameters are as given in Table II.

the detection of a theoretically predicted waveform can be calculated.

For the canonical burst waveform, Eq. (1), direct evaluation of Eq. (15) is possible with the result that

$$(S/N)_{I,\text{burst}}=\frac{h_0}{\tilde{h}}\left[\frac{N_{\text{hc}}\pi}{\omega_g}\right]^{1/2}, \tag{16}$$

and the SNR for detecting a waveform with fixed h_0 increases as the square root of the observation time, as set by the burst.

Similarly, the signal-to-noise ratio for the detection of the chirp waveform defined by Eq. (9) can be evaluated. Because the waveform has no (practical) beginning the observation is assumed to start when the source is emitting radiation at the frequency $f_{\min}$, and continues until coalescence. The integral in Eq. (15) is straightforward after averaging over the high-frequency behavior of Eq. (9) by replacing $h^2(\tau)$ with $\frac{1}{2}h_{\text{amp}}{}^2(\tau)$ and

$$(S/N)_{I,\text{chirp}}=\frac{1}{\tilde{h}}\frac{1}{R}\frac{\sqrt{5}\pi^{-2/3}G^{5/6}}{2\sqrt{2}c^{3/2}}F^{1/2}f_{\min}{}^{-2/3}. \tag{17}$$

As can be seen here, it is desirable to choose the lowest possible value for $f_{\min}$ to obtain a high SNR for detection. In practice the value of $f_{\min}$ will be set by the noise spectrum of the interferometer. Present-day interferometers invariably show a deviation from the flat white-noise spectrum at low frequencies as seismic noise sources overtake the laser shot noise.[4,18] If this colored noise has an $f^{-2/3}$ or steeper dependence (in fact f^{-3} is typical), then little improvement in the SNR for a detection can be made by observing the chirp at frequencies lower than this noise corner frequency.

V. BAR: MODEL AND RESPONSE

The detection of transient gravitational waves by a bar antenna is *conceptually* a two-step process. The gravitational wave interacts with the bar to deposit energy in the bar on a time scale short compared to the natural decay time of bar oscillations. Then, a transducer system monitors the bar's oscillations and data analysis operations are performed to search for changes in the bar's state of oscillation. The sensitivity of the transducer system is specified by the rms value of bar energy fluctuations that can be detected; kT_d. If an energy kT_s is deposited by the gravitational signal into the bar, then the *amplitude* SNR for its detection is given by

$$(S/N)_B=\left[\frac{T_s}{T_d}\right]^{1/2}. \tag{18}$$

Much research effort has gone into modeling and reducing the value of T_d;[20,21] however, here T_d is taken as a given instrumental parameter in the same way that $\tilde{h}$ is for the interferometer analysis of Sec. IV. Thus, the eval-

TABLE I. Summary of SNR results.

(a) Response to a general waveform $h(t)$:

$$(S/N)_B=\frac{1}{T_d{}^{1/2}}\frac{M_a{}^{1/2}L_a}{\pi^2k^{1/2}}\left[\left[\int\ddot{h}(t)\sin\omega_a t\,dt\right]^2+\left[\int\ddot{h}(t)\cos\omega_a t\,dt\right]^2\right]^{1/2}$$

$$(S/N)_I=\frac{1}{\tilde{h}}\left[2\int h^2(t)dt\right]^{1/2}$$

(b) Response to a burst parametrized by ϵMc^2, N_{hc}, and f_g, and R:

$$(S/N)_{B,\text{burst}}=\frac{1}{T_d{}^{1/2}}\frac{1}{R}\left[\frac{4\epsilon MG}{\pi kc}\right]^{1/2}M_a{}^{1/2}L_aN_{\text{hc}}{}^{1/2}f_g{}^{1/2}C\left[\frac{f_a}{f_g},N_{\text{hc}}\right]$$

$$(S/N)_{I,\text{burst}}=\frac{1}{\tilde{h}}\frac{1}{R}\left[\frac{2\epsilon MG}{\pi c}\right]^{1/2}f_g{}^{-1}$$

$$\frac{(S/N)_{B,\text{burst}}}{(S/N)_{I,\text{burst}}}=\frac{\tilde{h}}{T_d{}^{1/2}}\frac{\sqrt{2}}{\sqrt{k}}M_a{}^{1/2}L_aN_{\text{hc}}{}^{1/2}f_g{}^{3/2}C\left[\frac{f_a}{f_g},N_{\text{hc}}\right]$$

(c) Response to a chirp parametrized by $F=\mu m_T{}^{2/3}$ and R:

$$(S/N)_{B,\text{chirp}}=\frac{1}{T_d{}^{1/2}}\frac{1}{R}\frac{2\sqrt{5}G^{5/6}}{\sqrt{6k}\,\pi^{2/3}c^{3/2}}M_a{}^{1/2}L_aF^{1/2}f_a{}^{5/6}$$

$$(S/N)_{I,\text{chirp}}=\frac{1}{\tilde{h}}\frac{1}{R}\frac{\sqrt{5}\pi^{-2/3}G^{5/6}}{2\sqrt{2}c^{3/2}}F^{1/2}f_{\min}{}^{-2/3}$$

$$\frac{(S/N)_{B,\text{chirp}}}{(S/N)_{I,\text{chirp}}}=\frac{\tilde{h}}{T_d{}^{1/2}}\frac{4}{\sqrt{3k}}M_a{}^{1/2}L_af_a{}^{5/6}f_{\min}{}^{2/3}$$

uation of the SNR for a given $h(t)$ waveform requires a determination of T_s for that waveform. In this section the equivalent T_s for energy deposited in the bar is calculated for the burst and chirp waveforms.

The response of a bar antenna to a gravitational waveform is modeled using a harmonic-oscillator equivalent[22,23] which has an equation of motion given by

$$m_a\ddot{x}+m_a\omega_a{}^2x=F_g(t)=\tfrac{1}{2}m_a l_a\ddot{h}(t) \tag{19}$$

with

$$m_a=M_a/2\ ,$$

$$l_a=L_a\frac{4}{\pi^2}\ ,$$

$$\omega_a=2\pi f_a\ ,$$

where m_a and l_a are the effective mass and length of the bar antenna, M_a and L_a are the actual mass and length of the cylindrical antenna, and f_a is its resonant frequency. Note that a damping term has not been included because the duration of the signal is assumed to be much shorter than the ring-down time of the bar. It is straightforward to show that the energy deposited in the harmonic oscillator by the gravitationally induced force is

$$E_s=kT_s=\frac{1}{2m_a}\left[\left[\int F_g(t)\sin\omega_a t\,dt\right]^2+\left[\int F_g(t)\cos\omega_a t\,dt\right]^2\right]. \tag{20}$$

Substituting for F_g from Eq. (19) and using Eq. (18), the SNR for a detection is given in terms of $\ddot{h}(t)$ by

$$(S/N)_B=\frac{1}{T_d{}^{1/2}}\frac{M_a{}^{1/2}L_a}{\pi^2k^{1/2}}\left[\left[\int\ddot{h}(t)\sin\omega_a t\,dt\right]^2+\left[\int\ddot{h}(t)\cos\omega_a t\,dt\right]^2\right]^{1/2}, \tag{21}$$

where the bracketed term is just the Fourier amplitude of $\ddot{h}(t)$ at ω_a.

Using the formalism above, the signal-to-noise ratio for the detection of the canonical burst waveform of Sec. II can be calculated by substituting the $\ddot{h}(t)$ of Eq. (2) into Eq. (21) above, yielding

$$(S/N)_{B,\text{burst}}=\frac{1}{T_d{}^{1/2}}\frac{1}{2\pi k^{1/2}}M_a{}^{1/2}L_aN_{\text{hc}}\omega_g h_0\times C\left[\frac{\omega_a}{\omega_g},N_{\text{hc}}\right], \tag{22}$$

where

$$C\left[\frac{\omega_a}{\omega_g},N_{\text{hc}}\right]=\frac{\sin x}{x}\pm\frac{\sin y}{y}\mp\frac{4}{\pi N_{\text{hc}}}\times\begin{cases}\cos\left[\dfrac{\omega_a}{\omega_g}\dfrac{\pi N_{\text{hc}}}{2}\right]\\ \sin\left[\dfrac{\omega_a}{\omega_g}\dfrac{\pi N_{\text{hc}}}{2}\right]\end{cases} \tag{23}$$

with

$$x=\frac{\pi N_{\text{hc}}}{2}\left[1-\frac{\omega_a}{\omega_g}\right],$$

$$y=\frac{\pi N_{\text{hc}}}{2}\left[1+\frac{\omega_a}{\omega_g}\right],$$

and

upper of first and third choices for N_{hc} odd ,

upper of second choice for $N_{\text{hc}}=1,2,5,6,\ldots$.

Note that $C(1,N_{\text{hc}})$ is equal to unity and thus the "tuned," i.e., $\omega_a=\omega_g$, response of the bar is a simple expression. Because the energy flux of the incoming gravita-

TABLE II. SNR results for specific parameters.

(a) Detector parameters (circa 1985)

Interferometer (30 m)	Bar (4.2 K)
$\tilde{h}=2\times10^{-19}/\sqrt{\text{Hz}}$	$T_d=20$ m K
$f_{\min}=500$ Hz	$f_a=840$ Hz
	$L_a=3.0$ m
	$M_a=4.8\times10^3$ kg

(b) SNR's for burst sources with parameters
$\epsilon Mc^2=0.01M_\odot c^2$
$R=3\times10^{20}$ m $\simeq10$ kpc

$$(S/N)_{B,\text{burst}}=2.9N_{\text{hc}}{}^{1/2}\left[\frac{f_g}{840\text{ Hz}}\right]^{1/2}C\left[\frac{840\text{ Hz}}{f_g},N_{\text{hc}}\right]$$

$$(S/N)_{I,\text{burst}}=1.1\frac{840\text{ Hz}}{f_g}$$

$$\frac{(S/N)_{B,\text{burst}}}{(S/N)_{I,\text{burst}}}=2.7N_{\text{hc}}{}^{1/2}\left[\frac{f_g}{840\text{ Hz}}\right]^{3/2}C\left[\frac{840\text{ Hz}}{f_g},N_{\text{hc}}\right]$$

(c) SNR's for chirp sources with parameters
$R=3\times10^{20}$ m $\simeq10$ kpc
$F_\odot=M_\odot{}^{5/3}=(2\times10^{30}\text{ kg})^{5/3}$

$$(S/N)_{B,\text{chirp}}=3.5\times\left[\frac{F}{F_\odot}\right]^{1/2}$$

$$(S/N)_{I,\text{chirp}}=1.1\times\left[\frac{F}{F_\odot}\right]^{1/2}$$

$$\frac{(S/N)_{B,\text{chirp}}}{(S/N)_{I,\text{chirp}}}=3.2$$

tional wave is proportional to $\omega_g{}^2 h_0{}^2$, $C^2(\ )$ can be interpreted as the change in cross section of the bar as a function of the gravity-wave parameters.

For the chirp waveform the SNR is again given by Eq. (21); however, an exact analytic treatment is difficult because of the form of $\omega_g(t)$ and $\ddot{h}(t)$. The integrations can, however, be performed numerically and the process viewed graphically. The numerical results are shown in Fig. 3, where the waveform $\ddot{h}(t)$, the integrands of Eq. (21), and the partial evaluation of Eq. (21) (expressed as a temperature $T_{\rm bar}$) are plotted as a function of τ for several values of the source parameter F. The bar frequency f_a is 840 Hz in all cases and other source and bar parameters are as in Sec. VI. As is expected from Eq. (14) the number of cycles in the $\ddot{h}(t)$ waveform above the bar frequency decreases with increasing F. Also noticeable here is the finite period during which energy is deposited into the bar, given roughly by that section of the waveform which has a fixed phase relation to a sine wave at the bar frequency.

As these numerical results suggest, especially Fig. 3(a), a simplified analytic treatment is possible; the treatment here follows that presented by Clark and Eardley.[15] The waveform of Eq. (10) is expanded about the time τ_0 leading to the analytically more attractive form

$$\ddot{h}(t)=h_{\rm amp}(\tau_0)\omega_0{}^2 \sin\left[\omega_0 t+\frac{1}{2}\frac{d\omega}{dt}\bigg|_{\tau_0} t^2\right], \tag{24}$$

where $\omega_0=\omega_g(\tau_0)$. The phase of the waveform will have deviated appreciably from $\omega_0 t$ when the t^2 term in Eq. (24) contributes $\pi/2$ to the phase. This allows the definition of

$$q\equiv\text{radians until a }\frac{\pi}{2}\text{ phase shift}$$
$$=\frac{\pi^{1/2}\omega_0}{(d\omega/dt)^{1/2}}\ . \tag{25}$$

Thus, the time scale over which energy is deposited into the bar is given by

$$\Delta t\equiv\text{time until a }\frac{\pi}{2}\text{ phase shift}$$
$$=\frac{q}{\omega_0}$$
$$=2^{1/3}\left[\frac{5\pi}{24}\frac{c^5}{G^{5/3}}\right]^{1/2} F^{-1/2}\omega_0{}^{-11/6}\ , \tag{26}$$

where $d\omega/dt$ has been obtained from differentiation of Eq. (5) and Eq. (5) has been used to express the results as a function of ω_0. Values of Δt from this equation are indicated in Fig. 3 and show good agreement with the numerical results.

If q is large, as in Fig. 3(a), the integrals of Eq. (21) can be well approximated using the waveform of Eq. (24) and expanding around the bar frequency $\omega_0=\omega_a$. The resulting integrands of Eq. (21) are of the form $\sin\omega_a t\sin(\omega_a t+\alpha t^2)$ and $\cos\omega_a t\sin(\omega_a t+\alpha t^2)$. Using trigonometric identities and averaging over the high-frequency terms at $2\omega_g$, the SNR for a chirp detection becomes

$$(S/N)_{B,\rm chirp}=\frac{1}{T_d{}^{1/2}}\frac{M_a{}^{1/2}L_a}{\pi^2 k^{1/2}}h_{\rm amp}(\omega_a)\omega_a{}^2$$
$$\times\left\{\left[\frac{1}{2}\int_{-\infty}^{+\infty}\cos\left[\frac{1}{2}\frac{d\omega}{dt}t^2\right]dt\right]^2+\left[\frac{1}{2}\int_{-\infty}^{+\infty}\sin\left[\frac{1}{2}\frac{d\omega}{dt}t^2\right]dt\right]^2\right\} \tag{27}$$

and the resulting integrations are the familiar Cornu spiral integrals. These can be evaluated and result in a bar SNR for chirp detection of

$$(S/N)_{B,\rm chirp}=\frac{1}{T_d{}^{1/2}}\frac{M_a{}^{1/2}L_a}{2\pi^2 k^{1/2}}$$
$$\times h_{\rm amp}(\omega_a)\omega_a{}^2\pi^{1/2}\left[\frac{d\omega}{dt}(\omega_a)\right]^{-1/2}\ . \tag{28}$$

Further algebraic manipulations using Eqs. (5) and (6) allow us to express $d\omega/dt$ and $h_{\rm amp}$ as functions of ω_g and finally give

$$(S/N)_{B,\rm chirp}=\frac{1}{T_d{}^{1/2}}\frac{M_a{}^{1/2}L_a}{k^{1/2}}$$
$$\times\frac{1}{R}\frac{\sqrt{5}\times 2^{1/6}}{\sqrt{6}\pi^{3/2}}\frac{G^{5/6}}{c^{3/2}}F^{1/2}\omega_a{}^{5/6}\ . \tag{29}$$

The results of this simple formula, converted to temperature, are shown by the labeled horizontal lines in Fig. 3. Because this formula assumes an observation from the infinite past to the infinite future, the numerical results "Cornu oscillate" about this analytic asymptotic value. (Note that the final amount of energy deposited in the bar is very sensitive to the exact wave shape at the end of the chirp waveform.) However, agreement for F values where q is large is very good, and even at the extremes, where many of the assumptions are poorly met, Eq. (29) provides useful order-of-magnitude estimates.

VI. COMPARISON

The SNR results of the previous sections are in Table I according to the type of source and antenna. The SNR equations for detecting the constant energy bursts have been obtained by combining Eq. (4) with Eq. (16) or Eq. (22) as appropriate. The ratio of bar SNR to interferometer SNR has also been calculated and presented here. The expressions of Table I are evaluated for the operating parameters of the 4.2-K Stanford bar[2,24] and the MPQ Garching 30-m interferometer[18] with the results shown in Table II along with the parameters used. These two antennas have been chosen for comparison because they each represent the best performance of their respective antenna types (as of 1985) and their operation and performance are well documented. The SNR estimates for other detectors can be obtained by evaluating the equations of

Table I directly or by scaling the results of Table II.

Because of the frequency dependence of $C(\ )$, Eq. (23), the comparison of burst SNR values in Table II is valid only when the gravitational burst frequency f_g is equal to the bar antenna frequency f_a and represents a favorable case for the bar antenna. To compare the antennas for bursts at arbitrary frequency, the SNR's of Table I are plotted in Fig. 4 for several values of N_{hc} and a continuous range of f_g. As can be seen here, larger values of N_{hc} produce a larger SNR for bar detection but over a smaller range of burst frequency. The interferometer SNR for detecting constant gravitational energy bursts is independent of N_{hc} and shows a simple f^{-1} frequency dependence. The interferometer curve is discontinued below $f_{min}=500$ Hz, where $\tilde{h}$ increases from its shot-noise level as seismic noise sources become dominant.

The comparison of SNR sensitivities for the chirp sources produces the interesting result that the ratio of bar to interferometer SNR's of Table I are independent of the source parameter $F=\mu m_T^{2/3}$. However, the actual values of the SNR's for the antennas are a function of F and are plotted in Fig. 5, with R taken as 10 kpc. The curves have been discontinued at large values of F because of the calculational requirement that at f_a (or f_{min}) at least of order 5 cycles of the chirp waveform remain as given by Eq. (14). Thus, the subset of binary systems to which an antenna is (calculably) sensitive is limited by this requirement. For sources with F larger than the limiting value, the waveform, as far as the antennas are concerned, is not a chirp and its detection would be better analyzed as

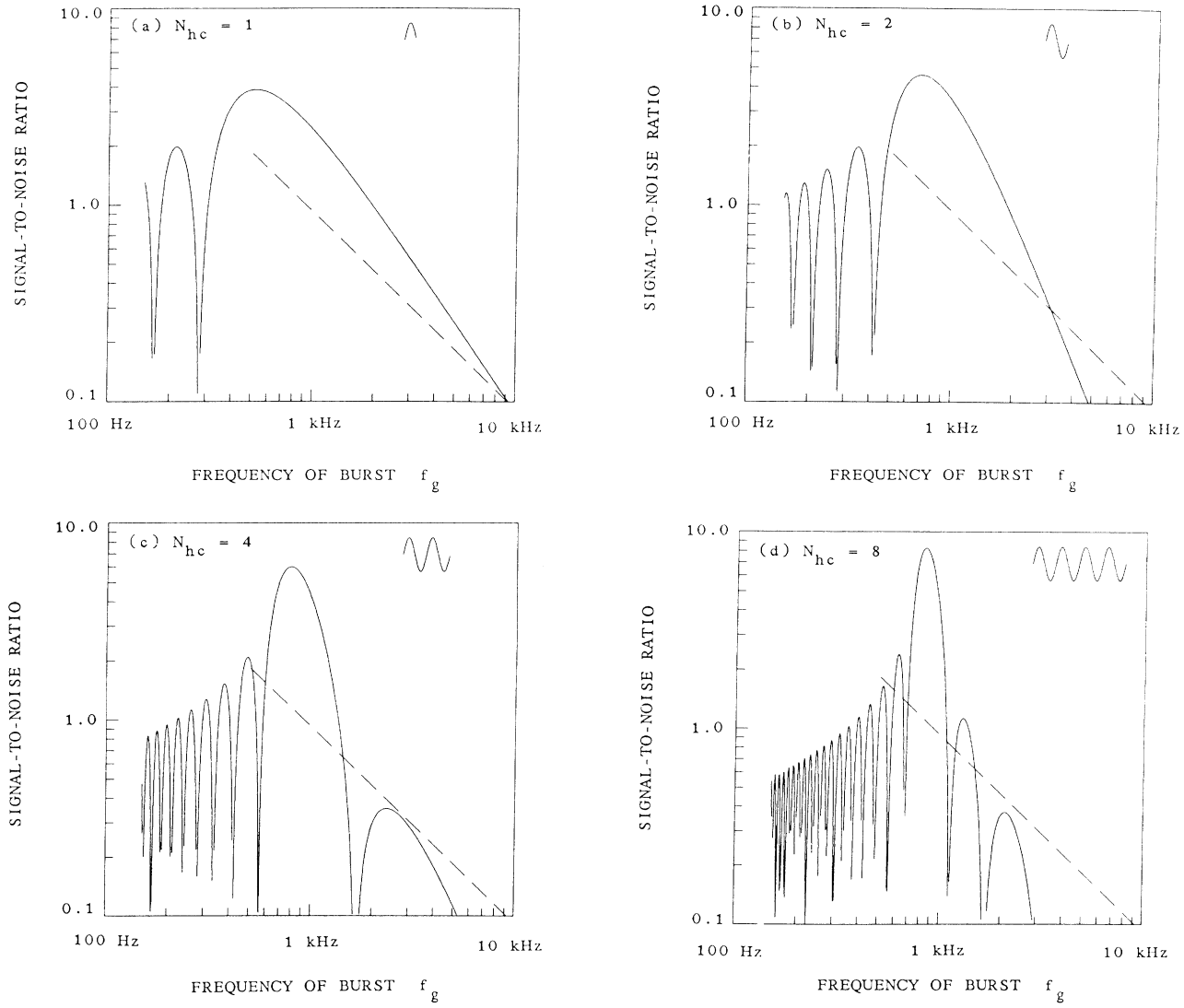

FIG. 4. Signal-to-noise ratios (SNR's) for detection of the canonical burst waveforms as a function of the emission frequency f_g for several values of N_{hc}. The 4.2-K Stanford bar SNR is given by the solid curves; the MPQ Garching 30-m interferometer SNR is given by the dashed lines. The source is located at a distance of 10 kpc and the total emitted gravitational wave energy is held constant at $10^{-2}M_{\odot}c^2$. The "narrow-banding" of the bar response for increasing N_{hc} is apparent. These results were computed from the equations in Table I using the antenna and source parameters summarized in Table II.

that of a burst. To indicate what systems are accessible to present-day antennas, Fig. 6 shows lines of constant F plotted in m_1,m_2 space and indicates the region in which the detectors are sensitive; in particular, the prototype system PSR1913+16 with $m_1=m_2=1.4M_\odot$ can be detected by either antenna.

Finally, we note that the near equality (within 20%) of the numerical values of $(S/N)_B/(S/N)_I$ for chirp and burst source detection could have been expected in order of magnitude but is otherwise due to evaluating the SNR's for $f_g=f_a$ and the instrumental coincidence that $f_{\min}$ is of the order of f_a.

VII. DISCUSSION

The results presented here allow a realistic comparison to be made of the sensitivities of the bar and interferometric antennas applied to the detection of transient sources. For the detection of burst sources, the canonical waveform of Fig. 2 provides a useful input for comparison of the frequency responses of the antennas. The response curves of Fig. 4 are representative of the tuned nature of the bar and the predicted gravity-wave sources. It is interesting that the bar response is as broad as it is, and the use of only a few bars tuned at different frequencies will ensure the detection of most burst events.

For the detection of chirp sources the results here have some clear implications for interferometer detection and indicate that more thought and perhaps some trade-offs are needed in the case of bar detection. For the interferometer a reduction of the seismic-shot-noise crossover frequency $f_{\min}$ both increases the SNR for the detection of the events and expands the region of detectable systems in m_1,m_2 space. For the bar, taking the SNR equation at face value indicates that improving the SNR for detection through increasing the bar resonant frequency f_a is at odds with covering a larger range of systems by decreasing f_a. However, the bar antenna is a complicated system and changing f_a cannot be done without changes in other parameters, in particular, the bar length L_a and the effective noise temperature T_d. Thus, the optimization of bar parameters for chirp detection will require further investigation.

The absolute values of the calculated SNR's of Sec. VI show that the Stanford bar and MPQ Garching interferometer are operating at comparable sensitivity levels and, furthermore, that these levels are promising for galactic astrophysics. In a coincidence experiment involving these two detectors, the Garching interferometer could provide a useful veto on the several-degree events seen occasionally by the Stanford bar.[24]

If information beyond source existence is desired or if sources as distant as the Virgo cluster are to be detected, SNR's ten to ten thousand times greater than those of these antennas are required. Thus, effort is going into reducing the values of $\tilde{h}$ and T_d of the antennas. For the interferometers, $\tilde{h}$ is given by the ratio $\delta\tilde{l}_{\rm opt}/Nl$ where $\delta\tilde{l}_{\rm opt}$ is the noise in measuring the optical phase shift (displacement) of the laser beam, N is the number of traversals of the interferometer arm made by the light, and l is the interferometer baseline. Extension of the baseline

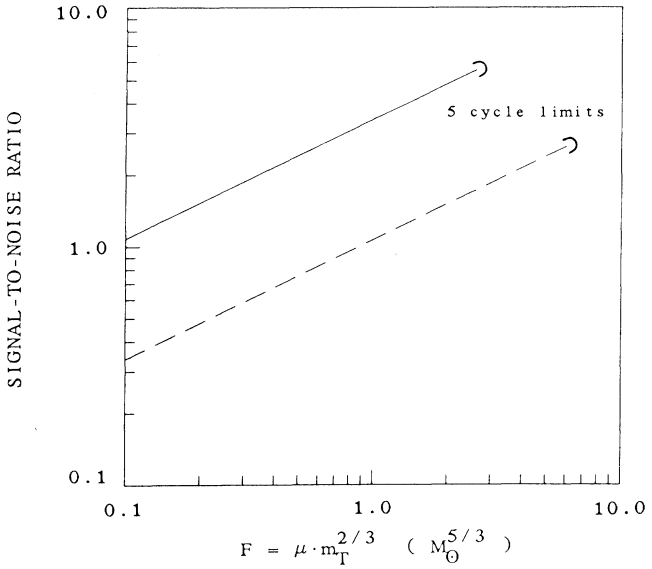

FIG. 5. Signal-to-noise ratios (SNR's) for detection of the chirp waveform emitted by a binary compact object system as a function of the source parameter F, with the source located at a distance of 10 kpc. The 4.2-K Stanford bar SNR is given by the solid line; the MPQ Garching 30-m interferometer SNR is given by the dashed line. The curves are discontinued at large F where too few cycles (<5) of the chirp waveform remain for the analytic calculations to be accurate. The equations of Table I and the parameters of Table II have been used for these calculations.

from the current 30 m (with $N=110$) to several kilometers[25,26] (with $N\sim30$) will allow an "immediate" improvement in SNR by a factor of 30. Additional improvements will come with increased laser power, reducing $\delta\tilde{l}_{\rm opt}$ by the square root of the power increase, and, for chirp

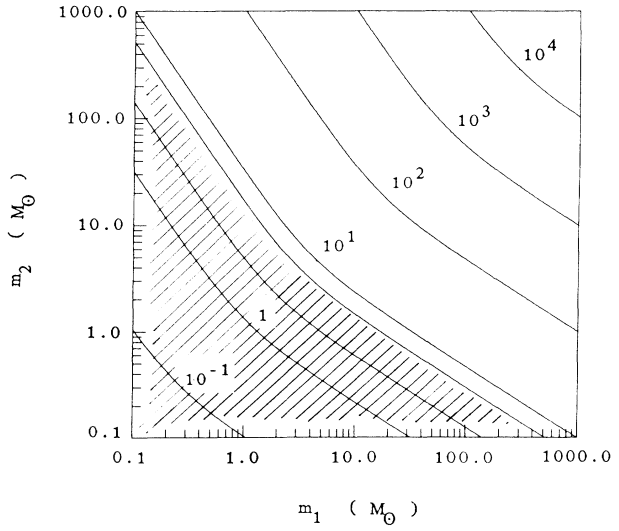

FIG. 6. Contours of constant F in m_1,m_2 space. The contours for $F=2.7$ and $F=6.4$ indicate the maximum F values for systems detectable by a bar with $f_a=840$ Hz and an interferometer with $f_{\min}=500$ Hz, respectively. The shaded region is that range of m_1,m_2 parameters accessible to the interferometer.

detection, through improved seismic isolation aimed at reducing $f_{\min}$ to 100 Hz or less.

For the bar antennas SNR improvements will go as the square root of reduction in the effective noise temperature T_d; T_d is proportional to the physical temperature of the bar T_a, inversely proportional to the Q of the bar, and depends on the bandwidth of the bar-transducer system. In addition to cooling next generation bars to a fraction of a degree and increasing Q values from 5×10^6 to the 10^8 range, advances leading to bar-transducer systems with larger bandwidths will provide the desired increases in the bar SNR. With these transducer improvements 4.2-K bar antennas with T_d less than 1 m K are already feasible.[21]

Finally, it should be pointed out that the primary desire here has been to understand the sensitivities of current antennas in several well-defined cases in which waveforms and antenna parameters can be explicitly given. Thus, geometric details and effects (such as averaging over source parameters and taking into account the antenna locations and orientations) have been left out for the sake of a clean comparison. These details are, however, important when considering a complete gravitational-wave detector system. For such a system, with multiple antennas at a variety of locations, these details must be included in making estimates of the expected astrophysical event rate, of the degree of sky coverage, and of the ability of the system to determine source locations and polarization properties.

ACKNOWLEDGMENTS

I gratefully acknowledge helpful discussions with P. F. Michelson, J. P. Richard, P. R. Saulson, and D. H. Shoemaker. Thanks to A. T. Patera for providing computational resources. This work was supported in part by the National Science Foundation under Grant No. 85-04836-PHY.

[1]J. Weber, Phys. Rev. **117**, 306 (1960).
[2]M. Bassan, W. M. Fairbank, E. Mapoles, M. S. McAshan, P. F. Michelson, B. Moskowitz, K. Ralls, and R. C. Taber, in *Proceedings of the Third Marcel Grossmann Meeting on General Relativity,* edited by H. Ning (North-Holland, Amsterdam, 1983), p. 667.
[3]R. L. Forward, Phys. Rev. D **17**, 379 (1978).
[4]R. Weiss, MIT Res. Lab. Electron. **105**, 54 (1972).
[5]H. Billing, K. Maischberger, A. Rüdiger, R. Schilling, L. Schnupp, and W. Winkler, J. Phys. E **12**, 1043 (1979).
[6]J. H. Taylor and J. M. Weisberg, Astrophys. J. **253**, 908 (1982).
[7]W. H. Press and K. S. Thorne, in *Annual Review of Astronomy and Astrophysics,* edited by L. Goldberg (Annual Reviews, Palo Alto, 1972), p. 355.
[8]S. L. Detweiler, in *Sources of Gravitational Radiation,* edited by L. Smarr (Cambridge University Press, Cambridge, England, 1979), p. 211.
[9]R. F. Stark and T. Piran, Phys. Rev. Lett. **55**, 891 (1985).
[10]Y. Kojima and T. Nakamura, Prog. Theor. Phys. **72**, 494 (1984).
[11]K. Oohara and T. Nakamura, Prog. Theor. Phys. **71**, 91 (1984).
[12]R. Saenz and S. Shapiro, Astrophys. J. **244**, 1033 (1981).
[13]R. Saenz and S. Shapiro, Astrophys. J. **221**, 286 (1978).
[14]R. L. Forward and D. Berman, Phys. Rev. Lett. **18**, 1071 (1967).
[15]J. P. A. Clark and D. M. Eardley, Astrophys. J. **215**, 311 (1977).
[16]L. D. Landau and E. M. Lifshitz, *The Classical Theory of Fields* (Pergamon, Oxford, 1975).
[17]B. Schutz, Nature **323**, 310 (1986).
[18]D. Shoemaker, W. Winkler, K. Maischberger, A. Rüdiger, R. Schilling, and L. Schnupp, in *Proceedings of the Fourth Marcel Grossmann Meeting on General Relativity,* edited by R. Ruffini (Elsevier, Amsterdam, 1986), p. 605.
[19]D. Dewey, in *Proceedings of the Fourth Marcel Grossmann Meeting on General Relativity* (Ref. 18), p. 581.
[20]P. F. Michelson and R. C. Taber, Phys. Rev. D **29**, 2149 (1984).
[21]J. P. Richard, J. Appl. Phys. **60**, 3807 (1986).
[22]E. Amaldi, in *Gravitational Radiation, Collapsed Objects and Exact Solutions,* proceedings of the Einstein Centenary Summer School, Perth, Australia, 1979, edited by C. Edwards (Lecture Notes in Physics, Vol. 124) (Springer, Berlin, 1980), p. 246.
[23]G. W. Gibbons and S. W. Hawking, Phys. Rev. D **4**, 2191 (1971).
[24]S. P. Boughn, W. M. Fairbank, R. P. Giffard, J. N. Hollenhorst, E. R. Mapoles, M. S. McAshan, P. F. Michelson, H. J. Paik, and R. C. Taber, Astrophys. J. **261**, L19 (1982).
[25]The MIT-Caltech large antenna plans are briefly described in Phys. Today **39** (2), 17 (1986).
[26]W. Winkler, K. Maischberger, A. Rüdiger, R. Schilling, L. Schnupp, and D. Shoemaker, *Proceedings of the Fourth Marcel Grossmann Meeting on General Relativity* (Ref. 18), p. 621.